



Advanced Materials and Manufacturing Processes

SCIENCE, TECHNOLOGY, AND MANAGEMENT



Edited by

**Amar Patnaik, Malay Kumar Banerjee, Ernst Kozeschnik,
Albano Cavaleiro, J. Paulo Davim, and Vikas Kukshal**

8 Study and Prediction of Response Parameters during Oblique Machining for Different Machining Parameters by WEDM of Inconel-HX

IV Manoj and S Narendranath

Taylor & Francis

CONTENTS

8.1	Introduction: Background and Driving Forces	119
8.2	Material.....	121
8.3	Experimental Technique and Parameters.....	121
8.4	Analysis of CV and SR.....	122
8.5.1	ANOVA and Main Effects Plot.....	123
8.5	Optimization at Each Angle Using Genetic Algorithm	125
8.6	Influence of WEDM at the Highest CV	127
8.7	Prediction of CV and SR Using ANFIS and ANN	128
8.8	Conclusion	131
	References.....	131

8.1 INTRODUCTION: BACKGROUND AND DRIVING FORCES

Nickel-based alloys have low thermal diffusivity and high-temperature strength. This makes the machining of these alloys very challenging [1–2]. Nontraditional machining like wire electric discharge machining (WEDM) was found to be an ideal process that can machine precision components made of these materials [3]. The complexity of the components demands different shapes in machining with good surface quality. Taper/oblique parts can be produced using WEDM by a unique way of bending the wire during machining. This traditional method causes many problems like inaccuracies, wire break and improper flushing, among others [4–6]. Yan et al. [7], Martowibowo and Wahyudi [8] and Manoj et al. [9–11], among other

researchers, have tried different mechanisms, materials and methods to improvise the traditional tapering in WEDM. Abbasi et al. [12] have explored the effects of pulse-on time, discharge gap, pulse ratio, discharge current and wire speed on surface integrity. Camposeco-Negrete [13] investigated that servo voltage affects on machining time, and the surface was influenced by pulse-off time. There was a decrease of 1.16% in surface roughness and 7.50% in machining time found by multi-objective optimization. Kumar et al. [14] studied surface roughness, material removal rate and kerf width, which was optimized with the aid of the grey relation analysis method. Ishfaq et al. [15] analyzed that 20% of cutting speed can be improved by optimizing the effects of layer thickness, workpiece orientation, dielectric pressure ratio, and wire diameter during the machining of stainless-clad steel. Nain et al. [16] stated that pulse-on time influences the wire-wear ratio, cutting speed and dimensional deviation. Chaubey and Jain [17] stated with the increase in pulse-off time, the surface roughness decreases. The cutting speed at different parameters also affected the surface roughness. Ishfaq et al. [18] employed a genetic algorithm to get the best permutation which derived minimum surface roughness at optimal cutting speed and a kerf width in WEDM of Al6061–7.5% silicon carbide (SiC) composite. Altug et al. [19] explored the outcome of different heat-treated Ti6Al4V by electric discharge machining. It was established that the genetic algorithm optimized parameters generated minimum kerf. Sivaprakasam et al. [20] have used the genetic algorithm optimization technique for optimal conditions, yielding minimum kerf width and surface roughness and maximum material removal rate. Chen et al. [21] employed the genetic algorithm for optimization of machining gap and material removal rate. The results were validated by experiments with prediction errors of 6.70% and 8.38% for the machining gap and material removal rate, respectively. Phate and Kumar et al. [22] have used prediction models devised by an artificial neural network (ANN) and dimensional analysis in WEDM of Al/SiC_p metal matrix composite (MMC). ANN models gave precise results in the prediction of surface roughness and material removal rate. Naresh et al. [23] investigated the adaptive neuro-fuzzy system (ANFIS) and ANNs prediction of responses in the machining of Nitinol alloy, it was established that the ANFIS predictor was most accurate. Abhilash and Chakradhar [24] have examined the causes of wire breakage and variation in mean gap voltage instances during machining of Inconel 718 by WEDM. ANFIS was used to foresee the wire-breakage situations, and the model shows the variations between input and output parameters. Riahi-Madvar and Seifi [25] have predicted gravel beds in rivers using ANN and ANFIS, in which it was concluded that ANFIS was superior to ANN in prediction.

The surface roughness (SR) and cutting velocity (CV) are essential factors that control the productivity and quality of machined components. These factors also have to be explored and optimized in the case of the tapering operations in WEDM due to their applications. In the present study, a novel method using the slant type fixture was employed to obtain the taper component without bending the wire, thereby avoiding the disadvantage of traditional tapering. The machining was performed at different oblique/taper angles, namely 0°, 15°, and 30°. The effects of different parameters like wire feed, servo voltage, pulse-off time, and pulse-on time on CV and SR. The oblique angle in machining increases SR and decreases CV in overall

Proof aspects, but the effects of the parameters remained unaltered. The genetic algorithm was employed in the optimization of CV and SR during oblique machining at different angles. ANN and ANFIS were used in the prediction of SR and CV.

8.2 MATERIAL

Inconel-HX is also called Hastelloy-X. It is a wrought nickel base alloy known as turbine alloys. Due to its excellent mechanical properties, it can be used in aircraft, furnace, petrochemical, and chemical processing industries. The heat-treatment method of solution annealing was performed at 1175°C (2150°F) as received material. The energy dispersive spectroscopy (EDS) of Inconel-HX is as shown in Figure 8.1.

8.3 EXPERIMENTAL TECHNIQUE AND PARAMETERS

The WEDM of the make “ELPULS 15 CNC WEDM” from Electronica, Pune was employed in the machining of Inconel-HX. It is hard to machine an alloy that has various applications in the aerospace, chemical, marine, industrial furnace, die and tool areas. The 0.25-mm-diameter wire of zinc-coated copper and deionized water was used in machining. The peak current is 12 A, and the servo feed is 20 mm/min. The slant-type taper fixture made of an aluminum alloy was fixed to the WEDM table as shown in Figure 8.2a. The workpiece was locked in the rotating angular plate, where it was fixed to the necessary position. The angular plate was made to rotate at different angles from 0°, 15° and 30° as shown in Figure 8.2b. The input parameters like servo voltage, wire feed, pulse-on time and pulse-off time were employed for the investigation. The main difficulty in the study was selecting the input parameters that could machine in all three oblique angles. These parameters were chosen based on initial experiments and machining capabilities [11, 26]. An L₁₆

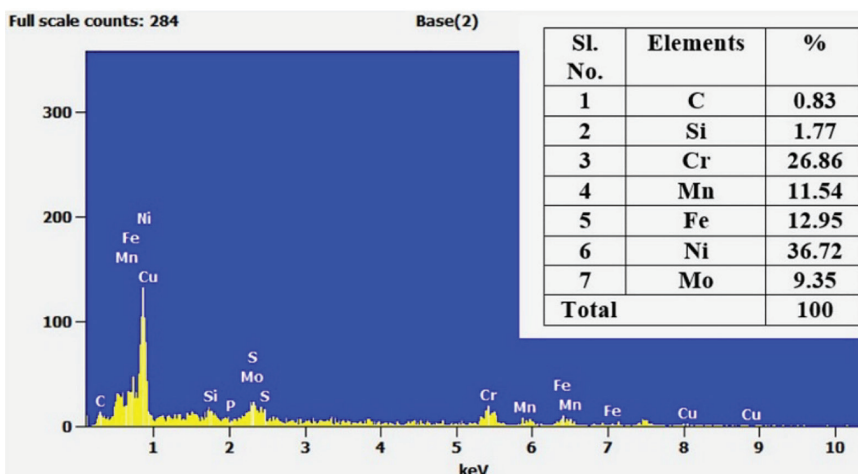


FIGURE 8.1 EDS of Inconel-HX.

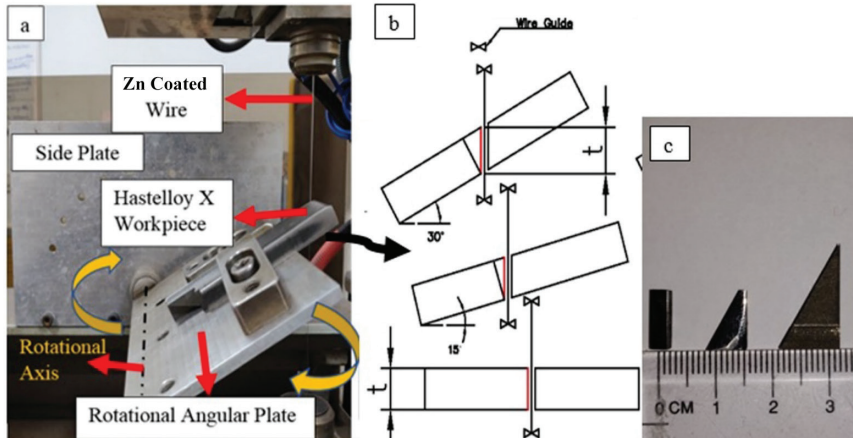


FIGURE 8.2 (a) Fixture used on WEDM (b) Oblique machining (c) WEDM-ed piece.

TABLE 8.1

Factors Considered for Experimentation

Factors	Phase 1	Phase 2	Phase 3	Phase 4
Pulse-on time (T_{on}) (μs)	110	115	120	125
Pulse-off time (T_{off}) (μs)	30	40	50	60
Servo gap voltage (SV) (V)	30	40	50	60
Wire feed (WF) (m/min)	5	6	7	8

Taguchi's orthogonal array was employed in which the CV and SR were recorded. The oblique machining was performed on Inconel-HX and Figure 8.2c shows components from the machining. The parametric variations were recorded, the CV was calculated as the average of instantaneous speed and the "Mitutoyo SJ-301" SR tester was employed for determining SR. Table 8.1 indicates the different steps employed for the parameters in the experimentation.

8.4 ANALYSIS OF CV AND SR

Table 8.2 illustrates the different parametric combinations used to the machine at different angles. It can be noticed that the highest CV obtained was 2.65 mm/min and 0.7 μm ; the lowest SR was recorded at 0°. The lowest CV was 0.13 mm/min and the highest SR of 4.27 μm at 30°. It was prominent that the CV decreases and SR increases as the oblique angle increases from 0° to 30°. This was due to the result of the growth in material thickness, which leads to improper flushing [24, 25]. The regression equations were formulated from Equations 8.1 through 8.6 by Minitab software.

TABLE 8.2
L₁₆ Orthogonal Array

Experiment No.	T _{on}	T _{off}	SV	WF	0°		15°		30°	
					CV	SR	CV	SR	CV	SR
1	110	30	30	5	1.58	1.93	1.43	2.31	1.28	2.71
2	110	40	40	6	1.32	1.33	1.17	1.71	1.02	2.11
3	110	50	50	7	0.82	0.89	0.77	1.13	0.62	1.53
4	110	60	60	8	0.79	0.70	0.28	0.92	0.13	1.32
5	115	30	40	7	1.88	2.47	1.73	2.74	1.58	3.14
6	115	40	30	8	1.79	2.76	1.64	3.11	1.49	3.51
7	115	50	60	5	0.90	0.95	0.75	1.22	0.60	1.62
8	115	60	50	6	0.98	1.04	0.83	1.34	0.68	1.69
9	120	30	50	8	2.15	2.63	2.05	2.93	1.90	3.28
10	120	40	60	7	2.14	1.53	2.04	1.73	1.89	2.08
11	120	50	30	6	2.40	3.59	2.30	3.89	2.15	4.24
12	120	60	40	5	1.59	2.22	1.49	2.52	1.34	2.87
13	125	30	60	6	2.22	2.13	2.12	2.43	1.97	2.78
14	125	40	50	5	2.48	3.32	2.38	3.67	2.23	4.02
15	125	50	40	8	2.65	3.19	2.55	3.54	2.40	3.94
16	125	60	30	7	2.54	3.62	2.44	3.87	2.29	4.27

Regression equations for CV and SR

$$CV \text{ at } 0^\circ = -3.14 + 0.0534 T_{\text{on}} - 0.02020 T_{\text{off}} - 0.00362 SV - 0.0567 WF \quad (8.1)$$

$$CV \text{ at } 15^\circ = -4.02 + 0.05542 T_{\text{on}} - 0.01273 T_{\text{off}} - 0.01257 SV - 0.0282 WF \quad (8.2)$$

$$CV \text{ at } 30^\circ = -5.314 + 0.07062 T_{\text{on}} - 0.01712 T_{\text{off}} - 0.01423 SV - 0.0271 WF \quad (8.3)$$

$$SR \text{ at } 0^\circ = -6.34 + 0.0729 T_{\text{on}} - 0.0012 T_{\text{off}} - 0.0133 SV + 0.044 WF \quad (8.4)$$

$$SR \text{ at } 15^\circ = -5.06 + 0.0877 T_{\text{on}} - 0.01430 T_{\text{off}} - 0.00552 SV + 0.0610 WF \quad (8.5)$$

$$SR \text{ at } 30^\circ = -4.49 + 0.0859 T_{\text{on}} - 0.01418 T_{\text{off}} - 0.05583 SV + 0.0672 WF \quad (8.6)$$

8.5.1 ANOVA AND MAIN EFFECTS PLOT

From Table 8.2, the main effects plot and analysis of variance (ANOVA) were derived by using Minitab software. At higher pulse-on times, the CV also increases, and a contrasting behavior was observed for the SV parameter. With the escalation in pulse-on time, the discharge energy increased across the electrode due to an escalation in spark intensity, and henceforth, this leads to higher melting at the wire-workpiece interface of the material. This increases the CV as observed in the literature [28, 29] and Figure 8.3a. At higher servo voltages, the gap between the job and the electrode is higher. This results in lower ionization, leading to fewer sparks and decreased discharge energy. Therefore, there is a decrease in CV as shown in Figure 8.3a. Regarding SR, it increases as pulse-on time escalates because of large-size craters found on the surfaces machined using WEDM. During higher pulse-on time, the discharge energy increases due to an escalation in the intensity of the spark.

This results in deeper and larger crater formations over the WEDM surface, in turn, increasing the SR as in Figure 8.3b. Similar results have been established by Kumar et al. [28]. But as servo voltage increases, there is a reduction in SR because of the escalation in the spark gap, which results in a lower spark intensity. This forms shallower and smaller craters on WEDM surface [28, 29]. Table 8.3 and Figures 8.3a and 8.3b both show that wire feed had low effects on the CV and SR. As the wire feed increases, the CV also increases, as the molten material formed was flushed out of the wire workpiece interface instantaneously. Due to this flushing action, a large number of the microcavities on the surface were formed, creating a higher surface finish [28]. At higher wire feed, there was a decrease observed in CV due to

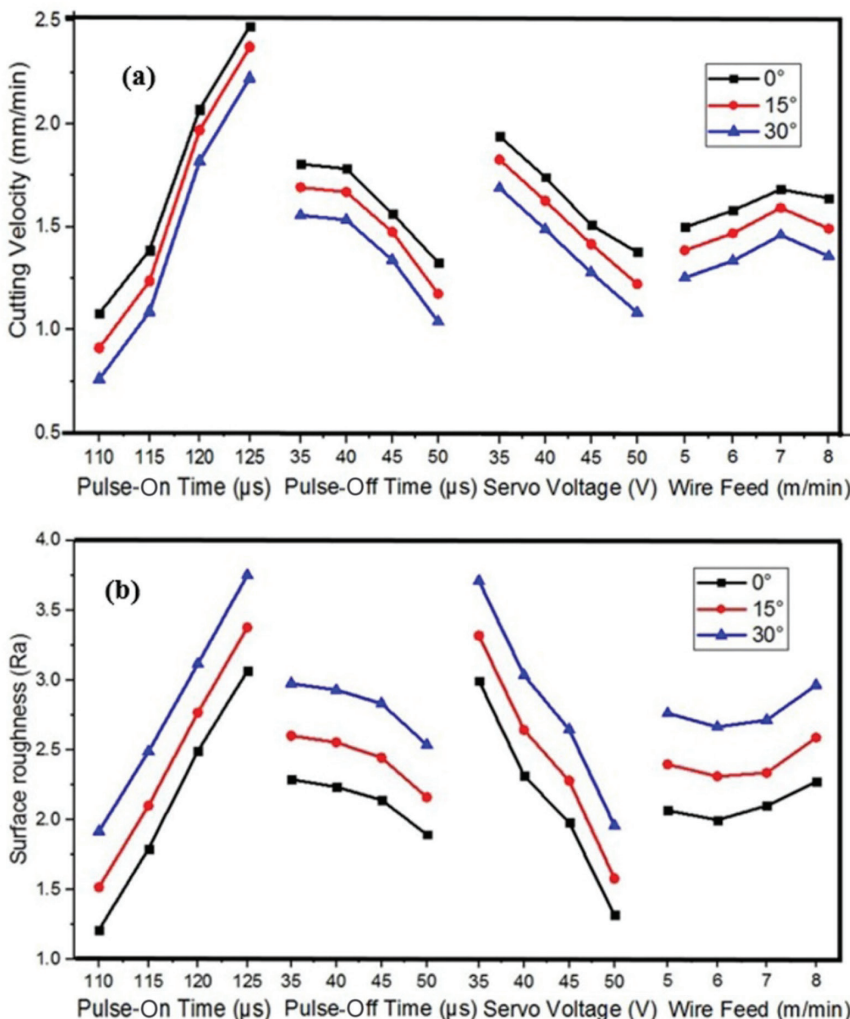


FIGURE 8.3 Effects Plot for (a) CV and (b) SR.

TABLE 8.3**ANOVA Indicating Percentage Contribution on Response Parameters**

Sl. No.	Source	DF	0°		15°		30°	
			Adj SS	% Contribution	Adj SS	% Contribution	Adj SS	% Contribution
CV								
1	T _{on}	3	4.819	72.11	5.065	73.88	5.342	72.62
2	T _{off}	3	0.735	11.00	0.705	10.28	0.843	11.46
3	SV	3	0.883	13.21	0.839	12.24	0.962	13.08
4	WF	3	0.097	1.45	0.120	1.75	0.109	1.48
5	Error	3	0.149	2.23	0.127	1.85	0.099	1.35
6	Total	15	6.683		6.856		7.356	
SR								
1	T _{on}	3	7.846	52.35	7.807	50.57	7.528	49.18
2	T _{off}	3	0.366	2.44	0.467	3.02	0.468	3.06
3	SV	3	5.735	38.26	6.179	40.02	6.302	41.17
4	WF	3	0.195	1.30	0.197	1.28	0.219	1.43
5	Error	3	0.846	5.64	0.791	5.12	0.789	5.15
6	Total	15	14.988		15.439		15.307	

the increase in wire vibration as shown in Figure 8.3a. Therefore, higher wire feed results in wire vibration [29]. In the case of SR, at higher wire feed, the SR increases. This was because of the wire vibration that occurs due to decreased tension at higher wire feeds. This leads to variations in the average spark gap, consequently increasing the SR as established by Chaudhary et al. [30]. In all the cases, the 30° angle shows lower CV and highest SR compared to 0° as stated in Section 8.5. The CV reduces as the oblique angle escalated because of the decrease in the melting of the material as in Figure 8.3. This phenomenon was observed because of the increase in material thickness that leads to better heat distribution as stated in Joy et al. [31]. In the case of the SR, the increased material thickness results in faster cooling of melted material on the WEDM surface as the dielectric fluid cools the material rapidly. So the SR escalates as established in the literature [26, 27] and depicted in Figure 8.3b.

8.5 OPTIMIZATION AT EACH ANGLE USING GENETIC ALGORITHM

This algorithm is a natural selection process whereby the fittest individuals/models/chromosomes are selected for reproduction to produce offspring of the succeeding generation. The genetic algorithm mainly works on three types of operators, namely, reproduction, crossover, and mutation. Reproduction mainly selects the best pair of chromosomes that was formed. This chromosome pair is improved monotonically from one generation to the next generation. The best chromosome pair is allowed for crossover with an assigned probable pair, which is generally good. This crossover introduces diversity in the gene pool by occasional random replacements

Proof

of other chromosomes. This leads to the creation of new chromosomes caused by the alteration (mutation), based on the crossovers. The chromosomes that possess high fitness in the gene pool among the parents and offspring are selected for the succeeding generation. The whole process is repeated to get the best combination [20]. The genetic algorithm facilitates the simultaneous optimization of two different parameters.

From earlier investigation, it is seen that there should be a trade-off in CV and SR. The conditions were

$$110 \leq T_{on} \leq 125, \quad (8.7)$$

$$30 \leq T_{off} \leq 60, \quad (8.8)$$

$$30 \leq V \leq 60, \quad (8.9)$$

$$5 \leq WF \leq 8. \quad (8.10)$$

The genetic algorithmic optimization was performed in a MATLAB environment using the optimization toolbox with parameters as shown in Table 8.4. It was seen that 110 (T_{on}), 56 (T_{off}), 58 (SV) and 6 (WF) were the optimal parameter set at all the three oblique angles. As seen in Table 8.5, the validated experimental results had a less than 5% error compared to the optimal predicted result.

Taylor & Francis
Not for distribution

TABLE 8.4
Genetic Algorithm Optimization Parameters

Sl. No.	Parameters	Values
1	Number of variables	4
2	Population	Double vector (size 50)
3	Function	Tournament (size 2)
4	Crossover segment	0.8
5	Probability in mutation	0.2
6	Generations	100
7	Stall generations	50

TABLE 8.5
Prediction and Experimental Validation of Optimized Results

Sl. No.	Oblique Angles (Degrees)	Experimental		Genetic Algorithm Optimization		% Error in CV	% Error in SR
		CV	SR	CV	SR		
1	0°	1.47	1.59	1.41	1.55	4.08	4.40
2	15°	1.12	1.9	1.10	1.81	1.79	4.74
3	30°	0.9	2.06	0.87	2.12	3.33	2.91

Proof

8.6 INFLUENCE OF WEDM AT THE HIGHEST CV

Figure 8.4 shows the scanning electron microscopy (SEM) images highlighting the change in average white-layer thickness (AWT) at the highest CV. During machining, the metal is melted and the molten metal is carried out in form of debris. The molten metal on the parent workpiece resolidifies to form a white layer on the WEDM surface. As the oblique angle rises, the AWT reduces due to better heat distribution. At higher oblique angles, the slant provided by the fixture increases the material thickness. This increase in thickness ensures better heat distribution, in turn, decreasing the thermal degradation [31]. This phenomenon was validated by microhardness (MH) testing at all the oblique angles. Figure 8.5 indications the change in MH at

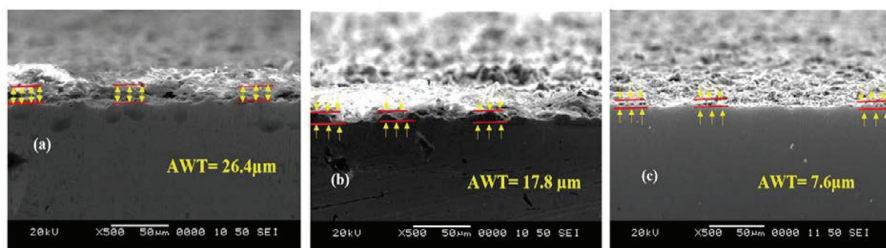


FIGURE 8.4 SEM Images at Different Oblique Angles: (a) 0°, (b) 15°, and (c) 30°.

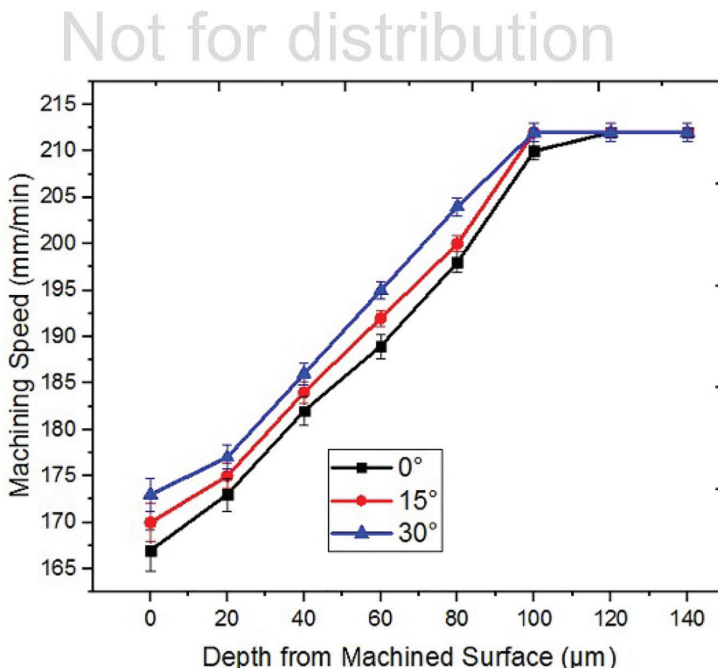


FIGURE 8.5 Variation of MH at Different Oblique Angles.

Proof

0° , 15° and 30° oblique angles. It was observed that higher oblique angles had lower MH; that is, the 30° oblique-angle WEDM surface showed 167HV MH. In the case of lower oblique angles, the MH was higher; that is, the 0° oblique-angle WEDM surface showed 173HV MH. The 15° oblique angle shows an AWT and MH to be between the 0° and 30° oblique angles.

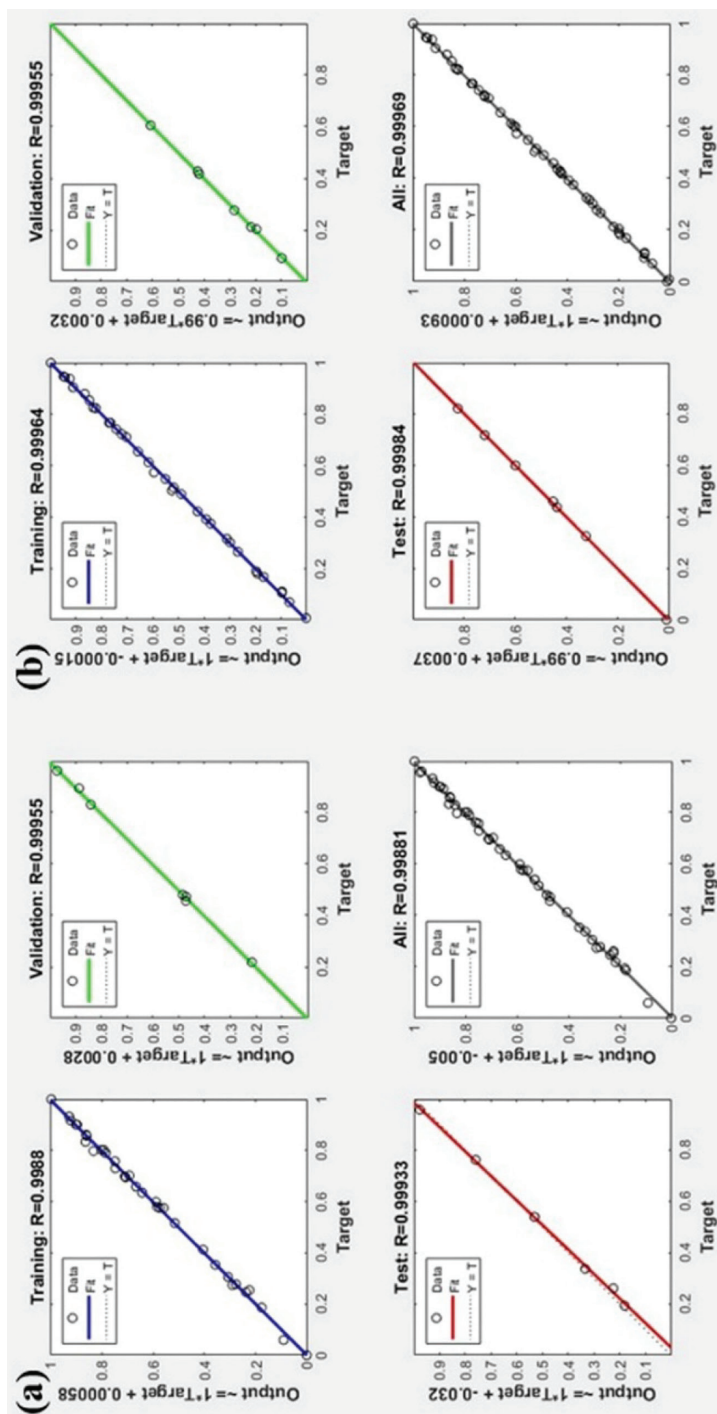
8.7 PREDICTION OF CV AND SR USING ANFIS AND ANN

From the earlier inferences, it was noticed that the oblique angle affects the response characteristics. So this was also considered as a parameter for the prediction of the output parameter. Forty-eight combinations of experiments were performed and used for the formulation of the optimum model in ANN and ANFIS. Figure 8.6 shows the regression plot generated during the training of the ANN model. The ANN and ANFIS models' parameters were set as shown in Table 8.6. Based on different trial experiments and literature [9, 23], these parameters were selected, and the optimal model was derived. From Figure 8.7, it can be noticed that the ANFIS model was better than the ANN model as the percentage error varied from 0–5% for both the response parameters. For the ANN model, it was observed that the error percentage varied from 0–10%. Figure 8.8 shows the actual mapping of input and output parameters. The three-dimensional plots show a better understanding of the actual variation in the output response with the machining parameters compared to the effects plots.

Not for distribution

TABLE 8.6
Modeling Parameters for ANN and ANFIS

Sl. No.	Network Parameters	Values
ANN		
1	Network structure	5-8-1-1
2	Training/validation/testing experimental sets	32/8/8 (48 experiments)
3	Algorithm used in network	Feedforward backpropagation
4	Transfer function	Tangential sigmoid
5	Function used for training	TRAINLM
6	Function for learning	LEARNGDM
7	Performance function	MSE
ANFIS		
1	Input parameters	48
2	Output parameters	1
3	Data used for training/testing	38/10
4	Input membership function	Gaussian
5	Output function	Constant
6	Fuzzy rules used in network	32 rules
7	Maximum epochs used	500/output



Proof

FIGURE 8.6 Regression Plots for (a) CV and (b) SR.

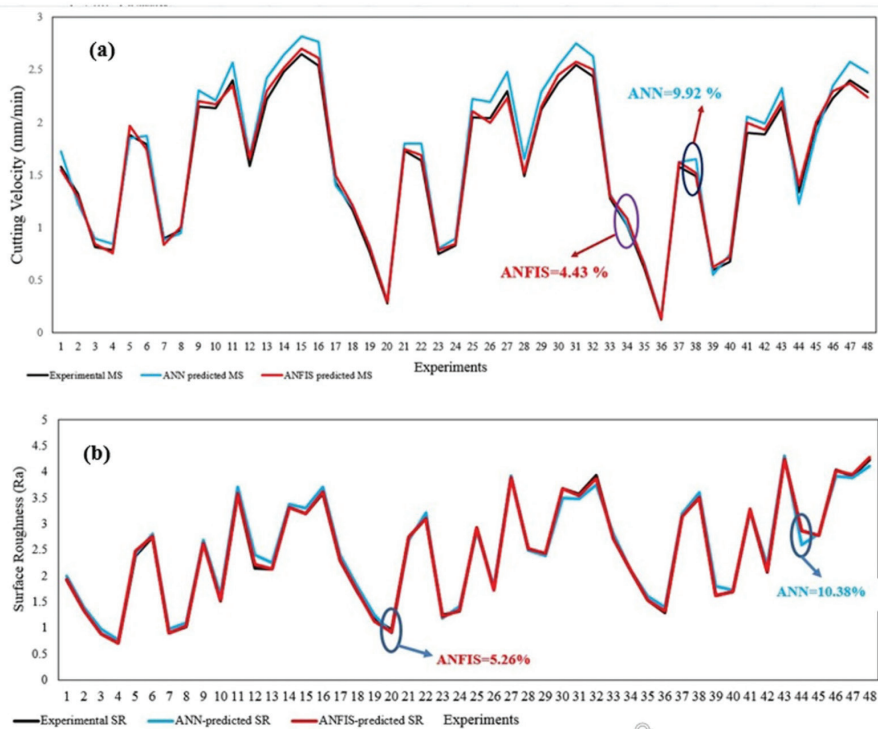


FIGURE 8.7 Experimental, ANN and ANFIS Prediction of (a) CV and (b) SR.

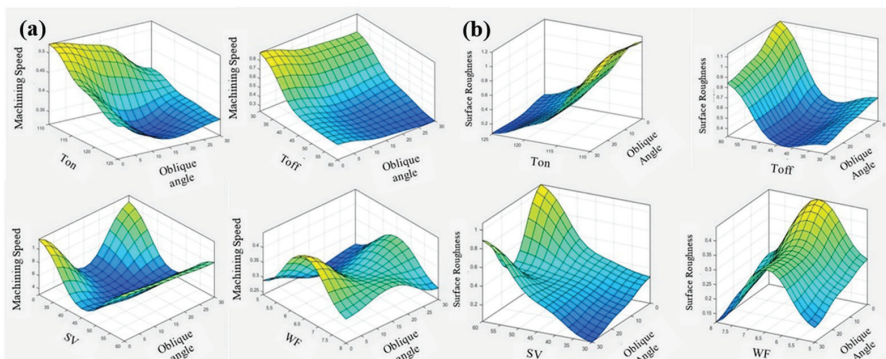


FIGURE 8.8 ANFIS Mapping for (a) CV and (b) SR

8.8 CONCLUSION

This research can be extended in the future to machining circular components without bending the wire as in the traditional process. The wire bending causes wire breakage, guide wear, improper flushing, angular inaccuracies, rough surface and the like. This study shows that oblique/taper machining of Inconel-HX was achieved by a unique angular placement of the workpiece with the aid of a fixture rather than the traditional technique. The effects of machining parameters on different responses for three oblique angles were analyzed, optimized, and predicted. The genetic algorithm used was validated experimentally, giving a less than 5% deviation. The pulse-on time affects both SR and CV. The response parameters increased with a rise in pulse-on time. The SR and CV reduce with an increase in servo voltage. The wire feed increases both SR and CV slightly. As machining is performed from 0° to 30° angles, the highest decrease of 83.54% in the CV and the highest increase of 71.91% in SR were observed. The AWT decreases whereas the MH increases at the WEDM surface at higher oblique angles. The ANFIS model was found to be most accurate in predicting the response parameters with a minimum-errors percentage ranging from 0–5%, and it also shows the variation of both input and output parameters by mapping.

REFERENCES

1. I.A. Choudhury, M.A. El-Baradie (1998) Machinability of nickel-base super alloys: a general review, *Journal of Materials Processing Technology*, 77, 278–284.
2. R. Arunachalam, M.A. Mannan (2000) Machinability of nickel-based high temperature alloys, *Machining Science and Technology, an International Journal*, 4, 127–168.
3. R. Maurya, R.K. Porwal (2020) EDM of Hastelloy—An overview, *Materials Today: Proceedings*, 26, 311–315.
4. N. Kinoshita, M. Fukui, T. Fujii (1987) Study on Wire-EDM: accuracy in taper-cut, *CIRP Annals—Manufacturing Technology*, 36,119–122. [https://doi.org/10.1016/S0007-8506\(07\)62567-0](https://doi.org/10.1016/S0007-8506(07)62567-0).
5. J.A. Sanchez, S. Plaza, L.N. Lopez De Lacalle, A. Lamikiz (2006) Computer simulation of wire-EDM taper-cutting, *International Journal of Computer Integrated Manufacturing*, 19, 727–735.<https://doi.org/10.1080/09511920600628855>.
6. S. Plaza, N. Ortega, J. A. Sanchez, I. Pombo, A. Mendikute (2009) Original models for the prediction of angular error in wire-EDM taper-cutting, *The International Journal of Advanced Manufacturing Technology*, 44, 529–538.
7. H. Yan, Z. Liu, L. Li, C. Li, X. He (2017) Large taper mechanism of HS-WEDM, *The International Journal of Advanced Manufacturing Technology*, 90, 2969–2977. <https://doi.org/10.1007/s00170-016-9598-9>.
8. S.Y. Martowibowo, A. Wahyudi (2012) Taguchi method implementation in taper motion wire EDM process optimization, *Journal of The Institution of Engineers (India): Series C*, 93, 357–364. <https://doi.org/10.1007/s40032-012-0043-z>.
9. I.V. Manoj, S. Narendranath (2020) Variation and artificial neural network prediction of profile areas during slant type taper profiling of triangle at different machining parameters on Hastelloy X by wire electric discharge machining, *Proceedings of the Institution of Mechanical Engineers, Part E: Journal of Process Mechanical Engineering*, 234, 673–683. <https://doi.org/10.1177/0954408920938614>.

Proof

10. I.V. Manoj, S. Narendranath (2021) Influence of machining parameters on taper square areas during slant type taper profiling using wire electric discharge machining, IOP Conference Series: Materials Science and Engineering, 1017, 1–9.
11. I.V. Manoj, R. Joy, S. Narendranath, D. Nedelcu (2019) Investigation of machining parameters on corner accuracies for slant type taper triangle shaped profiles using WEDM on Hastelloy X. IOP Conference Series: Materials Science and Engineering, 591, 1–11.
12. J. Ali Abbasi, M. Jahanzaib, M. Azam, S. Hussain, A. Wasim, M. Abbas (2017) Effects of wire-Cut EDM process parameters on surface roughness of HSLA steel, *The International Journal of Advanced Manufacturing Technology*, 91, 1867–1878. <https://doi.org/10.1007/s00170-016-9881-9>.
13. C. Camposeco-Negrete (2019) Prediction and optimization of machining time and surface roughness of AISI O1 tool steel in wire-cut EDM using robust design and desirability approach, *The International Journal of Advanced Manufacturing Technology*, 103, 2411–2422. <https://doi.org/10.1007/s00170-019-03720-3>.
14. A. Kumar, T. Soota, J. Kumar (2018) Optimisation of wire-cut EDM process parameter by Grey-based response surface methodology, *Journal of Industrial Engineering International*, 14, 821–829. <https://doi.org/10.1007/s40092-018-0264-8>.
15. K. Ishfaq, N.A. Mufti, M.P. Mughal, M.Q. Saleem, N. Ahmed (2018) Investigation of wire electric discharge machining of stainless-clad steel for optimization of cutting speed, *The International Journal of Advanced Manufacturing Technology*, 96, 1429–1443. <https://doi.org/10.1007/s00170-018-1630-9>.
16. S.S. Nain, D. Garg, S. Kumar (2018) Investigation for obtaining the optimal solution for improving the performance of WEDM of super alloy Udimet-L605 using particle swarm optimization, *Engineering Science and Technology, An International Journal*, 21(2), 261–273.
17. S.K. Chaubey, N.K. Jain (2018) Investigations on surface quality of WEDM-manufactured meso bevel and helical gears, *Materials and Manufacturing Processes*, 33, 1568–1577.
18. K. Ishfaq, S. Anwar, M. Asad Ali, M.H. Raza, M.U. Farooq, S. Ahmad, C.I. Pruncu, M. Saleh, B. Salah (2020) Optimization of WEDM for precise machining of novel developed Al6061–7.5% SiC squeeze-casted composite, *The International Journal of Advanced Manufacturing Technology*, 111, 2031–2049.
19. M. Altug, M. Erdem, C. Ozay (2015) Experimental investigation of kerf of Ti6Al4V exposed to different heat treatment processes in WEDM and optimization of parameters using genetic algorithm, *The International Journal of Advanced Manufacturing Technology*, 78, 1573–1583.
20. P. Sivaprakasam, P. Hariharan, S. Gowri (2014) Modeling and analysis of micro-WEDM process of titanium alloy (Ti6Al4V) using response surface approach, *Engineering Science and Technology, An International Journal*, 17, 227–235.
21. X. Chen, Z. Wang, Y. Wang, G. Chi (2020) Investigation on MRR and machining gap of micro reciprocated wire-EDM for SKD11, *International Journal of Precision Engineering and Manufacturing*, 21, 11–22.
22. M.R. Phate, S.B. Toney (2019) Modeling and prediction of WEDM performance parameters for Al/SiCp MMC using dimensional analysis and artificial neural network, *Engineering Science and Technology, an International Journal*, 22, 468–476.
23. C. Naresh, P.S.C. Bose, C.S.P. Rao (2020) Artificial neural networks and adaptive neuro-fuzzy models for predicting WEDM machining responses of Nitinol alloy: comparative study, *SN Applied Sciences*, 314, 1–23.
24. P.M. Abhilash, D. Chakradhar (2020) ANFIS modelling of mean gap voltage variation to predict wire breakages during wire EDM of Inconel 718, *CIRP Journal of Manufacturing Science and Technology*, 31, 153–164.

Proof

- Proof
25. H. Riahi-Madvar, A. Seifi (2018) Uncertainty analysis in bed load transport prediction of gravel bed rivers by ANN and ANFIS, Arabian Journal of Geosciences, 688, 1–20.
 26. I.V. Manoj, R. Joy, S. Narendranath (2020) Investigation on the effect of variation in cutting speeds and angle of cut during slant type taper cutting in WEDM of Hastelloy X, Arabian Journal for Science and Engineering, 45(2), 641–651. <https://doi.org/10.1007/s13369-019-04111-2>.
 27. A. Goswami, J. Kumar (2017) Trim cut machining and surface integrity analysis of Nimonic 80A alloy using wire cut EDM, Engineering Science and Technology, An International Journal, 20, 175–186.
 28. V. Kumar, V. Kumar, K.K. Jangra (2015) An experimental analysis and optimization of machining rate and surface characteristics in WEDM of Monel-400 using RSM and desirability approach, Journal of Industrial Engineering International, 11, 297–307.
 29. P. Sharma, D. Chakradhar, S. Narendranath (2015) Evaluation of WEDM performance characteristics of Inconel 706 for turbine disk application, Materials and Design 88, 558–566.
 30. T. Chaudhary, A.N. Siddiquee, A.K. Chanda (2019) Effect of wire tension on different output responses during wire electric discharge machining on AISI 304 stainless steel, Defence Technology, 15, 541–544.
 31. R. Joy, I.V. Manoj, S. Narendranath (2020) Investigation of cutting speed, recast layer and micro-hardness in angular machining using slant type taper fixture by WEDM of Hastelloy X, Materials Today: Proceedings, 27, 1943–1946.

Taylor & Francis
Not for distribution

Proof

Proof

Taylor & Francis
Not for distribution

Proof